J. Fluid Mech. (1996), *vol.* 328, *pp.* 19–48
Copyright © 1996 Cambridge University Press

The development of asymmetry and period doubling for oscillatory flow in baffled channels

By E. P. L. ROBERTS[1] AND M. R. MACKLEY[2]

[1] Department of Chemical Engineering, UMIST, PO Box 88, Manchester, M60 1QD, UK

[2] Department of Chemical Engineering, University of Cambridge, Pembroke Street, Cambridge, CB2 3RA, UK

(Received 18 May 1995 and in revised form 13 June 1996)

We report experimental and numerical observations on the way initially symmetric and time-periodic fluid oscillations in baffled channels develop in complexity. Experiments are carried out in a spatially periodic baffled channel with a sinusoidal oscillatory flow. At modest Reynolds number the observed vortex structure is symmetric and time periodic. At higher values the flow progressively becomes three-dimensional, asymmetric and aperiodic. A two-dimensional simulation of incompressible Newtonian flow is able to follow the flow pattern at modest oscillatory Reynolds number. At higher values we report the development of both asymmetry and a period-doubling cascade leading to a chaotic flow regime. A bifurcation diagram is constructed that can describe the progressive increase in complexity of the flow.

1. Introduction

The progressive transition of ordered flows to more complex flow structures is of significant academic and technological interest. In many cases the problem is examined by increasing the flow rate of a steady flow either in a plane channel or around a stationary obstacle. There is however considerable scope to introduce unsteadiness in either the fluid motion or movement of the solid boundary. In this paper we are concerned with an unsteady fluid motion, specifically a fully periodic oscillation of the volumetric flow rate. Many studies have been carried out with oscillations in smooth tubes, see for example Park & Baird (1970). In this case the transition from laminar to turbulent flow occurs at a high Reynolds number, of order 10000, as a rapid transition. In an obstructed geometry however (e.g. Stephanoff, Sobey & Bellhouse 1980; Sobey 1980; Brunold *et al.* 1989) the complexity of the flow develops at modest Reynolds numbers of order 100. At these modest Reynolds number the flow can be followed using numerical simulation as well as by experimental techniques, providing additional insight into the developing complexity of the flow.

These oscillatory flows can be characterized by a Strouhal number (St) and oscillatory Reynolds number (Re):

$$St = \Omega H/U, \tag{1}$$

$$Re = HU/\nu, \tag{2}$$

where Ω is the frequency of oscillation, H is a characteristic dimension, HU is the peak volumetric flow and ν is the kinematic viscosity of the fluid.

Sobey (1983) has shown that for laminar oscillatory flow in wavy-walled channels three distinct flow regimes can be identified.

(i) For large Strouhal numbers, $St > 0.1$, the flow field is dominated by viscosity.

(ii) For low Strouhal numbers, the flow behaves in a quasi-steady manner. Under these conditions the velocity field at any time t can be approximated by the velocity field obtained under steady flow conditions, for the same geometry and with a volumetric flow equal to that at time t in the oscillation cycle.

(iii) For intermediate Strouhal numbers, non-quasi-steady behaviour is observed. In this regime a sequence of vortex formation, growth during acceleration, and ejection upon flow reversal occurs during each oscillation. This process has been termed 'vortex mixing'.

Oscillatory flow in a wavy-walled channel has been studied using both numerical simulation and experimental flow visualization by Sobey (1980, 1983) and Stephanoff *et al.* (1980). In general the observed flows were symmetric about the channel centreline, periodic and exhibited space–time symmetry:

$$u(x, y, z, t) = -u(-x, y, z, t+\tfrac{1}{2}T), \tag{3a}$$

$$v(x, y, z, t) = v(-x, y, z, t+\tfrac{1}{2}T), \tag{3b}$$

$$w(x, y, z, t) = w(-x, y, z, t+\tfrac{1}{2}T), \tag{3c}$$

where T is the periodic of the oscillation. Ralph (1986) has studied oscillatory flow in a wavy-walled tube and found similar regimes to those described above for a wavy-walled channel. Ralph (1986) also observed that in a narrow band of St between regimes (i) and (iii) the flow exhibited increased complexity with greater vortex interaction. In particular he observed that under some conditions ($0.02 < St < 0.05$) the space–time symmetry of the flow was broken. Under these conditions the flows were observed to be periodic over one or more complete oscillation cycles, though in one case the flow was apparently aperiodic.

Nishimura *et al.* (1991) have also observed a breaking of the space–time symmetry for oscillatory flow in a wavy-walled channel for $0.02 < St < 0.0284$ and for $Re > 200$. The numerical simulations of Nishimura *et al.* (1991) suggested that these flows which exhibited this space–time asymmetry were also no longer spatially periodic in the x-direction over one cycle of the geometry. However, the spatial asymmetry observed was essentially a numerical error and its true cause was not established.

From a dynamical systems viewpoint oscillatory flow in an obstructed geometry might be considered to be analogous to a forced, damped nonlinear oscillator, with storage (kinetic energy) and loss (viscous dissipation) mechanisms. Although the system in this case does not exhibit a natural oscillation in the absence of oscillatory forcing, a natural oscillation can be observed with a steady flow (Roberts 1994). The transition from space–time symmetry to space–time asymmetry and subsequent higher-periodicity regimes may be considered to be a consequence of a bifurcation of this forced nonlinear dynamical system. Forced nonlinear oscillators such as the Duffing oscillator are known to show period doubling which leads to chaotic behaviour (e.g. Thompson & Stewart 1986). Analysis of the period-doubling behaviour of oscillatory flow from a dynamical systems perspective may provide further insight into these flow regimes.

Sobey (1985) has observed asymmetric (with respect to the channel centreline) flows for oscillatory flow in a symmetric sudden expansion. The asymmetry was observed to occur at oscillatory Reynolds numbers of order 100 and was in the form of a large-amplitude wave with successive counter-rotating vortices. A similar wave has been observed for channel flows with a moving indentation (Ralph & Pedley 1988).

Asymmetric oscillatory flows in periodically obstructed geometries have been observed experimentally in baffled tubes (Dickens, Mackley & Williams 1989; Hewgill *et al.* 1993) but have not been studied in detail.

The transitions in periodicity and symmetry described above merit more detailed attention in order to improve the understanding of the development of flow complexity.

The successive vortex ejection process that can be obtained in the non-quasi-steady regime also has engineering significance for the enhancement of mixing and transport processes. Bellhouse *et al.* (1973) reported the success of a membrane oxygenator using oscillatory flow across a furrowed membrane which indicated good surface mass transport under laminar flow conditions. More recently oscillatory flow in a baffled tube has been shown to provide a favourable plug-flow-like residence time distribution (Dickens *et al.* 1989), as well as enhanced heat transfer (Mackley, Tweddle & Wyatt 1990) and gas–liquid mass transfer rates (Hewgill *et al.* 1993).

The baffled tube geometry studied experimentally by Dickens *et al.* (1989) indicated that an amplitude of oscillation (centre to peak) of only 1 mm in a 25 mm diameter tube gives minimum dispersion. This corresponds to $St = 2.0$, which is an order of magnitude larger than the limiting St for vortex mixing determined by Sobey (1983) and Ralph (1986). Flow visualization photographs under these conditions (Dickens *et al.* 1989) indicate that vortex mixing is still occurring. This apparent contradiction is explained by considering that the sharp-edged baffles used by Dickens *et al.* (1989) force the flow to separate, ensuring that vortex mixing will occur at much higher Strouhal numbers than for the relatively smooth geometries of Sobey (1980, 1983) and Ralph (1986). Howes (1988) has studied oscillatory flow in a baffled tube geometry using both numerical simulation and experimental flow visualization. These results confirm that for this geometry vortex mixing is observed for Strouhal numbers up to $St \sim 4$. Howes (1988) also observed that under some conditions, for Strouhal numbers in the range 0.25–0.5, the space–time symmetry of the flow was broken.

This paper aims to study the developing complexity of oscillatory flow in a baffled rectangular channel. The observed periodicity behaviour and the transition to asymmetric flow are addressed using two-dimensional numerical simulation and flow visualization. The transition to three-dimensional flow is also studied using experimental flow visualisation. This geometry is suitable for the study of period-doubling behaviour over a range of Strouhal numbers. Furthermore, the transition from symmetric to asymmetric flow can be studied using a simple two-dimensional numerical simulation.

The paper is divided into six sections. In §2 the theoretical equations and numerical techniques are described. A brief description of the experimental flow visualization techniques is presented in §3. The observed flow patterns are described in §4. Section 5 discusses the influence of the numerical parameters on some of the features described in §4. The final section is a concluding discussion of the results described in the paper.

2. Theoretical equations and numerical techniques

The geometry studied is a periodically baffled channel as shown in figure 1. For simplicity a single set of geometric parameters is used, with a baffle height and spacing of $B = H/4$ and $L = 3H/2$ respectively. The flow is assumed to be two-dimensional in x and y, and periodic in x.

The flow modelling scheme used is based on the work of Sobey (1980) for furrowed channels and Howes (1988) for ducted tubes. The model has been used by Howes, Mackley & Roberts (1991) and Roberts (1994) and is described in detail by Roberts

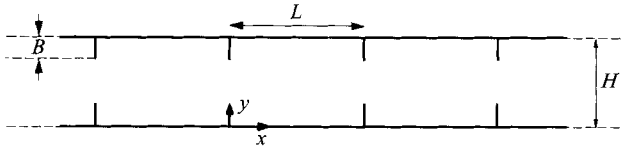

FIGURE 1. The baffled channel geometry showing the rectangular coordinate system. Geometric parameters are $B = H/4$ and $L = 1.5H$.

(1992). The numerical scheme is in the form of a vorticity–streamfunction finite-difference solver for an incompressible Newtonian fluid. The definition of a streamfunction restricts the model to two spatial dimensions. This approach has been used by Howes (1988) to study axisymmetric tube flow, while the results presented in this paper are two-dimensional channel flow, allowing the relaxation of the centreline symmetry constraint.

In the equations below, length has been made dimensionless with channel height H, velocities with peak mean oscillatory velocity $2\pi\Omega x_0$, and time with $1/\Omega$, where Ω is the frequency of oscillation (in Hz) and x_0 is the centre-to-peak amplitude of oscillation. The key equations used are the Poisson-type relationship between ω and ψ and the vorticity transport equation:

$$\omega = -\left(\frac{\partial^2\psi}{\partial x^2} + \frac{\partial^2\psi}{\partial y^2}\right), \tag{4}$$

$$\frac{\partial\omega}{\partial t} = -\frac{1}{St}\left(\frac{\partial(u\omega)}{\partial x} + \frac{\partial(v\omega)}{\partial y}\right) + \frac{1}{Re\,St}\left(\frac{\partial^2\omega}{\partial x^2} + \frac{\partial^2\omega}{\partial y^2}\right), \tag{5}$$

where Re is the oscillatory Reynolds number ($2\pi\Omega x_0 H/\nu$, where ν is the kinematic viscosity of the fluid) and St is the Strouhal number ($H/2\pi x_0$). For the geometry of figure 1 and for a sinusoidal oscillatory flow the boundary conditions for these equations are as follows:

(*a*) no slip at the walls:

$$u = v = 0 \quad \text{on all walls and baffles;} \tag{6}$$

(*b*) the total volumetric flow rate is equal to the difference in the streamfunction at the top and bottom walls:

$$\psi = 0.5\sin(2\pi t) \quad \text{on the top wall,} \tag{7}$$

$$\psi = -0.5\sin(2\pi t) \quad \text{on the bottom wall.} \tag{8}$$

The flow is also assumed to be spatially periodic with the flow in each cell identical. This assumption provides an additional boundary condition:

(*c*) spatial periodicity:

$$\psi_{x=L} = \psi_{x=0}, \tag{9}$$

$$\omega_{x=L} = \psi_{x=0}. \tag{10}$$

This is achieved numerically by substituting forwards and backwards the conditions at each end of the cell. Relaxation of this constraint is considered in §5.

The flow can be forced to be symmetric by solving one half of the domain of interest and using a centreline boundary condition:

$$\omega = \psi = 0 \quad \text{on the centreline.} \tag{11}$$

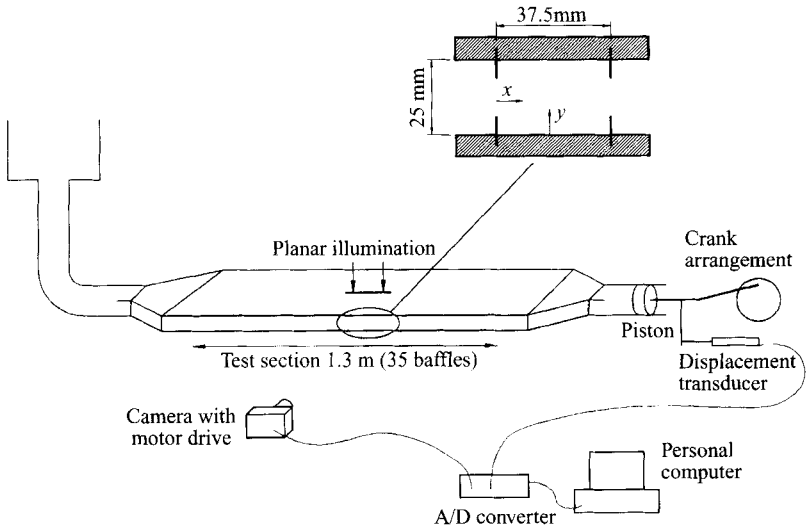

FIGURE 2. Schematic diagram of the experimental set-up. The orientation of the (x, y) coordinate system is shown in the enlarged cross-section. The set-up shown is for visualization of the flow patterns in the (x, y)-plane. For (x, z)-visualization the camera and illumination were rotated through 90° about the channel centreline, with the camera above the channel. The frequency and amplitude of the oscillation were determined on the personal computer, using the signal from the displacement transducer via the A/D converter. The camera shutter was driven from the A/D converter in order to take photographs at strategic points in the oscillation cycle.

Finite-difference versions of (4) and (5) form the base equations for the numerical simulation. The vorticity transport (5) is used to step forward in time and (4) is then solved for the streamfunction. Velocities (u, v) are obtained from the definition of the streamfunction. Centred differencing is used for accuracy and the explicit leapfrog method of Dufort & Frankel (see Roache 1976) is used for the time stepping of the vorticity transport equation. The length of the time step is chosen to retain numerical stability (based on the convective terms), and is typically 0.0025.

The finite-difference equations are solved on a regular array of grid points. Except where stated explicitly in the text a grid of 42 points in the x-direction ($x = 0$ to 1.5) and 65 points in the y direction ($y = 0$ to 1) is used. Grid refinement tests indicate that this grid size is sufficient to provide accuracy without requiring excessive computation. Some details of the effect of grid refinement on observed flow features are discussed in §5.

3. Experimental flow visualization

A diagram of the experimental apparatus is shown in figure 2. The experimental set-up has also been used for studying constant volumetric flow in a baffled channel and has been described by Roberts (1994). The test section consisted of a Perspex channel with periodically placed stainless steel baffles push fitted into the walls, arranged with y as the vertical coordinate. The channel height H was 25 mm and the baffle spacing L was 37.5 mm. The aspect ratio of the channel cross-section was 1:8, and the channel length was 1.3 m (34 baffles). The fluid used was a mixture of methylated spirits and water (60% by volume water, kinematic viscosity 2.535×10^{-6} m^2 s^{-1} at 20 °C).

Flow oscillations were provided using a 50 mm diameter piston driven by an offset crank arrangement, electric motor and gearbox. The crank arrangement could provide

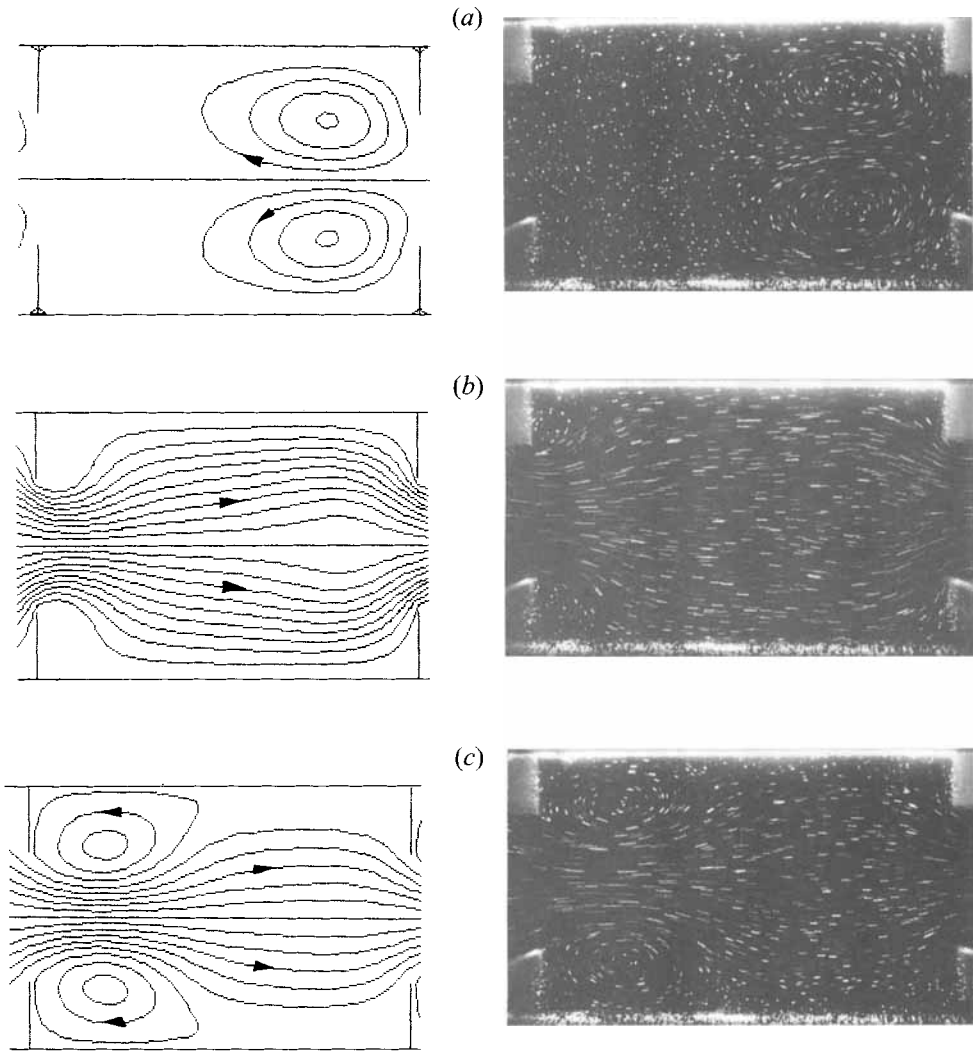

FIGURE 3(*a–c*). For caption see facing page.

peak to peak amplitudes of piston motion of 19.9, 29.9, 44.7 and 59.6 mm. These amplitudes correspond to Strouhal numbers in the test section of 1.0, 0.68, 0.453 and 0.341. The frequency of oscillation was varied between 0.1 and 2.2 Hz corresponding to an oscillatory Reynolds number in the range $50 < Re < 750$.

A mercury vapour lamp was used to provide planar illumination (in the x, y-plane) through a narrow slit ~ 3 mm wide at the centreline of the channel. In order to study cross-channel motions a horizontal plane of light (in the x, z-plane) close to the centreplane ($y = H/2$) of the channel was used. Light scattering was achieved with neutrally buoyant polyethylene particles having diameter of order 100 μm.

The flow patterns were observed using a 35 mm SLR stills camera and motor drive. Streakline photographs of the flow were taken with exposure times of between 1/30 and 1/4 s. In order to minimize entrance effects a cell at the centre of the test section was used for the streakline photographs. The position of the piston was monitored using a displacement transducer, A/D converter and personal computer. The A/D

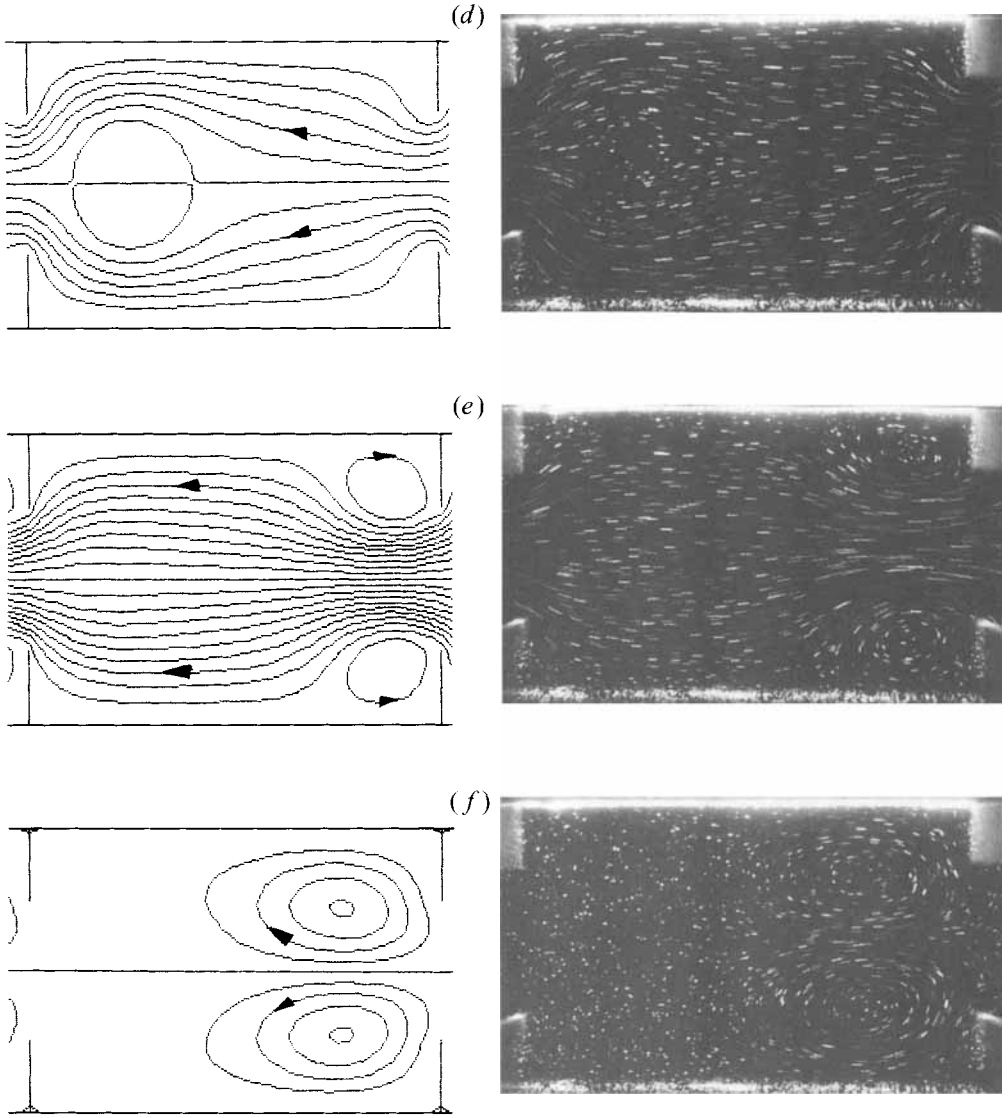

FIGURE 3. A sequence of observed flow patterns in the (x, y)-plane for one oscillation cycle. The right-hand figures show the experimental streakline photographs taken using a plane of light in the centre of the channel in the (x, y)-plane with an exposure time of 1/8 s. The left-hand figures show instantaneous plots of streamlines (constant streamfunction ψ at intervals of 0.05) obtained using a two-dimensional numerical simulation. The Reynolds number $Re = UH/\nu$ and Strouhal number $St = UH/\Omega$ based on the peak mean velocity U and the channel height H were 60 and 0.68 respectively. (*a*) $t = t_0$ (an integer), (*b*) $t = t_0 + 0.2$, (*c*) $t = t_0 + 0.4$, (*d*) $t = t_0 + 0.6$, (*e*) $t = t_0 + 0.8$, and (*f*) $t = t_0 + 1.0$.

converter was used to drive the camera so that streakline photographs could be taken at strategic points in the oscillation cycle, with an accuracy of around $\pm 2°$ (i.e. $\pm 0.6\%$ of the oscillation cycle time).

4. Observed flow patterns

Flow patterns from the numerical simulation are depicted using contour plots of the instantaneous streamfunction. Streakline photographs with a plane of light through the channel in the (x, y)-plane are compared with the numerically generated streamlines. Streakline photographs taken from above the channel with a plane of light (in the x, z-plane) close to the centreplane are used to establish the three-dimensional nature of the flow. Using this approach it is possible to identify the nature of the transition to three-dimensional flow. The regime under which the flow patterns are dominantly two-dimensional can be established for direct comparison with the two-dimensional simulation.

4.1. *Experimental observations*

Figure 3 is a sequence of streakline photographs showing motions in the (x, y)-plane using a vertical plane of light for oscillatory flow at $Re = 60$, $St = 0.68$. Also shown are plots of the numerically generated instantaneous streamlines for the equivalent time sequence. The flows show good agreement with the size and location of the eddies predicted by the simulation. The flow patterns are qualitatively similar to the flow patterns reported by Sobey (1980) for wavy-walled channels and Ralph (1986) for wavy-walled tubes. The sequence of vortex formation during acceleration, non-quasi-steady growth during deceleration and ejection on flow reversal is clearly evident. The Strouhal number is however considerably higher than the regimes studied in earlier works. As the flow is forced to separate by the sharp-edged baffle the vortex mixing behaviour can still be observed at these high Strouhal numbers. The flow patterns in figure 3 indicate that the flow is fully periodic over one oscillation. This is clear from comparison of figures 3(*a*) and 3(*f*). Further observations of the flow at successive flow reversals indicate that the flow exhibits space–time symmetry in this regime.

Figure 3 is typical of the flow patterns observed for Reynolds numbers $Re < 100$. In this regime good agreement between the experimental observations and the numerical simulation is observed for all Strouhal numbers studied. The flows are symmetric with respect to the channel centreline and also exhibit space–time symmetry. The strong pair of eddies evident at flow reversal (figure 3*a*) is observed to grow in strength and decrease in size with increasing Reynolds number. The effect of decreasing the Strouhal number is equivalent to increasing the displacement amplitude (x_0), and for a constant oscillatory Reynolds number the frequency of oscillation Ω will decrease. With decreasing Strouhal number the pair of eddies formed in the previous half-cycle of the oscillation increase in size (due to the increase in x_0) and decrease slightly in strength (due to the decrease in Ω). Flow patterns at a range of Reynolds number and Strouhal number in this regime have been published in a separate paper (Roberts & Mackley 1995).

4.1.1. *Transition to three-dimensional flow*

Experimental observations indicate that the flow becomes three-dimensional at an oscillatory Reynolds number of order 100 for all Strouhal numbers studied. Figure 4 shows the streakline pattern observed from above the channel with a horizontal plane of light (in the x, z-plane) close to the centreplane, for $Re = 60$, $St = 0.453$, at flow

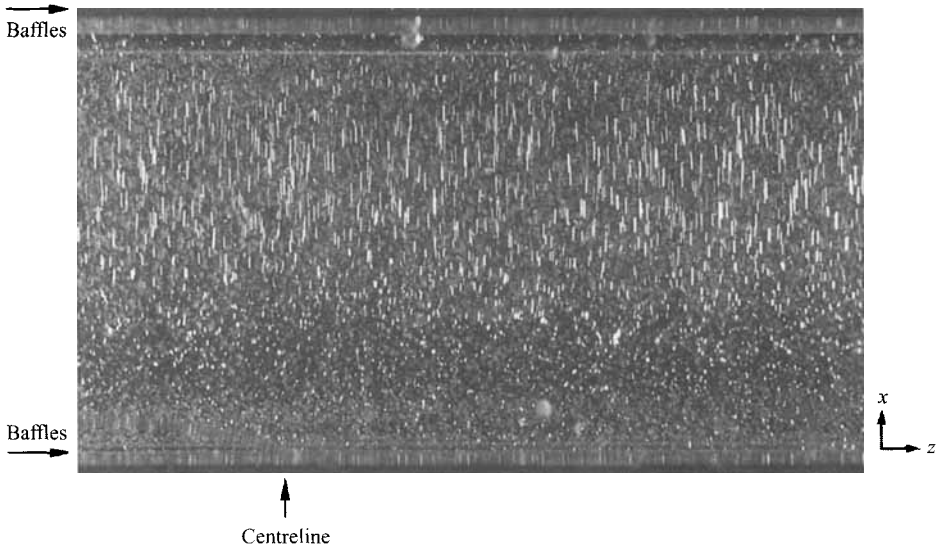

FIGURE 4. Streakline photograph showing a dominantly two-dimensional flow regime. The photograph was taken from above the channel at the point of flow reversal (t = an integer) using a plane of light in the (x, z)-plane just above the channel centreplane, with an exposure time of 1/4 s. The location of the baffles and the location of the channel centreline are marked on the figure. Re and St were 60 and 0.453 respectively.

reversal (t = an integer). Streaks associated with the eddy formed in the upper part of the channel during the last half-cycle are evident. Very little motion across the channel (in the z-direction) is apparent and the flow is dominantly two-dimensional. Figure 5 shows the same streakline pattern observed for a flow with $Re = 130$, $St = 0.453$, at two successive flow reversals. Structured cross-channel motions are clearly evident. A sequence of pairs of counter-rotating eddies is apparent and the flow is periodic through the depth of the channel. At the second flow reversal the flow is the mirror image, but with the eddies shifted across the channel. After one cycle (i.e. $t = t_0 + 1.0$, not shown) the flow is identical to figure 5(a), indicating that although the flow is three-dimensional it is fully repeating over one cycle. It is clear from figure 5(b) that the flow is not space–time symmetric in the sense of (3). However the flow patterns suggest that the flow may have a modified form of space–time symmetry, with

$$u(x, y, z, t) = -u(-x, y, z+\tfrac{1}{2}W, t+\tfrac{1}{2}T), \tag{12a}$$

$$v(x, y, z, t) = v(-x, y, z+\tfrac{1}{2}W, t+\tfrac{1}{2}T), \tag{12b}$$

$$w(x, y, z, t) = w(-x, y, z+\tfrac{1}{2}W, t+\tfrac{1}{2}T), \tag{12c}$$

where W is the wavelength of the instability in the z-direction.

Figure 6 shows the streakline pattern observed from above the channel for a flow with $Re = 300$, $St = 0.453$ at flow reversal (t = an integer + 0.5). The sequence of eddy pairs is no longer evident and the flow appears disordered with a range of eddy sizes and a chaotic three-dimensional structure.

This sequence of developing three-dimensional motion is observed for all values of Strouhal number studied. In all cases the flows appears to be two-dimensional for oscillatory Reynolds numbers below $\sim$ 100. Figure 5 and further observations of the

(*a*)

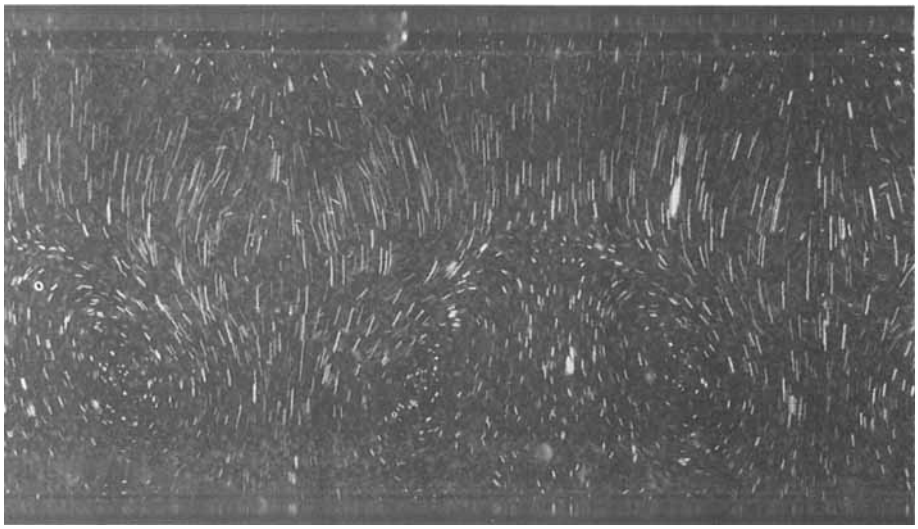

(*b*)

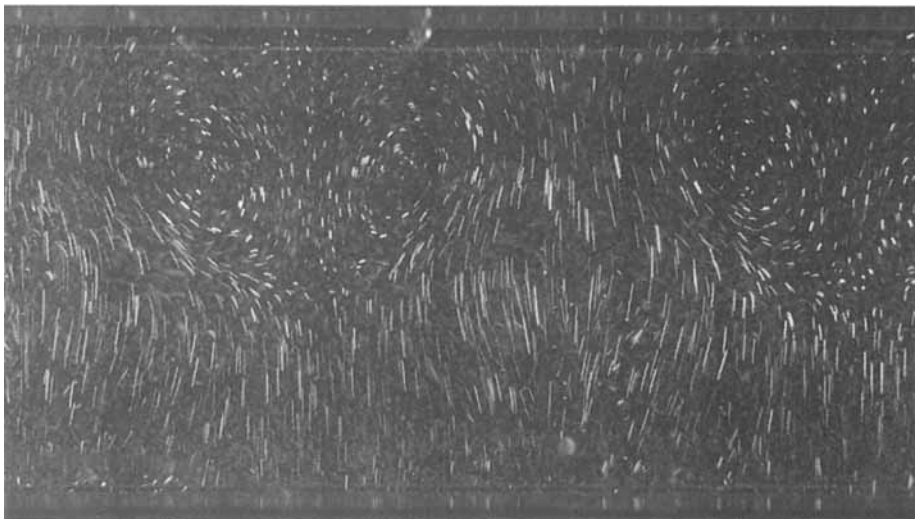

FIGURE 5. Streakline photographs showing the formation of a structured three-dimensional flow. The photographs were taken at two successive flow reversals using a plane of light in the (x, z)-plane just above the channel centreplane, with an exposure time of 1/8 s. The position of the baffles and the channel centreline are as shown in figure 4. *Re* and *St* were 130 and 0.453 respectively. (*a*) $t = t_0$ (an integer) and (*b*) $t = t_0 + 0.5$.

full channel width indicate that the sequence of eddies is apparently uniform across the channel. This would suggest that the transition to three-dimensional flow is due to a flow instability rather than the finite depth of the channel.

The size of the spanwise eddies observed in these structured flows decreases with decreasing Strouhal number. Table 1 shows the wavelength (W) estimated from the flow visualization photographs for the range of Strouhal number studied, with $Re = 130$.

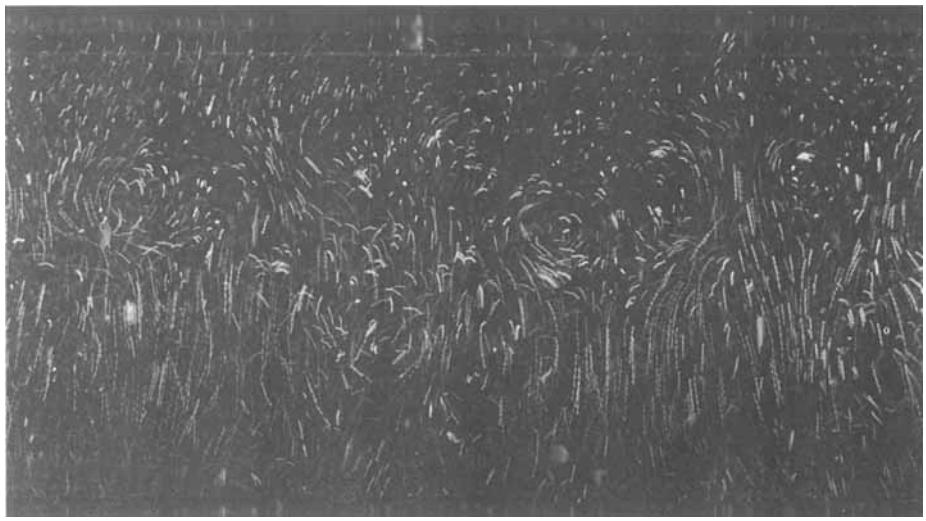

FIGURE 6. Streakline photograph showing a disordered three-dimensional flow. The photograph was taken at the point of flow reversal (t = an integer + 0.5) using a plane of light in the (x, z)-plane just above the channel centreplane, with an exposure time of 1/15 s. The position of the baffles and the channel centreline are shown in figure 4. Re and St were 300 and 0.453 respectively.

St	W/L
1.0	2.5
0.68	1.3
0.453	1.1
0.341	1.0

TABLE 1. The spanwise wavelength (W) of the three-dimensional instability for $Re = 130$

The three-dimensional flow structure apparent in figure 5 is similar to that observed by Nishimura *et al.* (1991) for oscillatory flow in wavy-walled channels. Careful observation of the flow in adjacent cells suggests that there is a phase shift of 180° in the cross-channel eddy structure between adjacent cells. This corresponds to the 'type A' instability observed by Nishimura *et al.* (1991) at higher Strouhal numbers. Although the magnitude of the Strouhal number studied here is considerably larger than that of Nishimura *et al.* (1991), the wavelengths shown in table 1 are of the same order of magnitude as the wavelengths observed by Nishimura *et al.* (1991) for the 'type A' instability: $W/L = 0.5$–1.2. However the trend of increasing wavelength with increasing Strouhal number is opposite to that observed by Nishimura *et al.* (1991).

Figure 7 shows a streakline photograph in the (x, y)-plane at flow reversal, for the same flow conditions as for figure 5 ($Re = 130$, $St = 0.453$). Crossed streaklines due to the finite thickness of the plane of light clearly indicate that the flow is three-dimensional, in agreement with figure 5. Some slight asymmetry is apparent in the flow though we believe this is caused by asymmetric imperfections of the geometry rather than a symmetry-breaking bifurcation. In general, oscillatory flow at this Reynolds number was found to be symmetric in the (x, y)-plane about the channel centreline.

Observations at successive flow reversals indicate that the space–time symmetry of the flow has been broken. Because of the three-dimensional structure however, the observed flow pattern is a function of the location of the plane of light (i.e. the z-

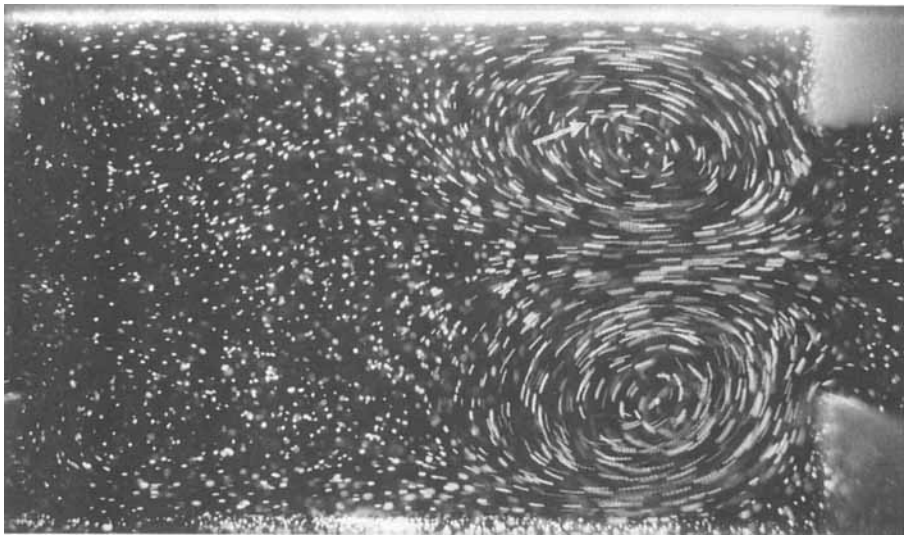

FIGURE 7. A streakline photograph showing the flow pattern in the (x, y)-plane for the flow conditions of figure 5. The presence of crossed streaklines (an example is indicated with an arrow on the figure) indicate that the flow is three-dimensional. The photograph was taken using a plane of light in the centre of the channel in the (x, y)-plane with an exposure time of 1/15 s. Re and St were 130 and 0.453 respectively.

coordinate). At some locations flows which appear to be space–time symmetric can be observed. However the (x, z) flow patterns (figure 5) clearly show that the three-dimensional flow is no longer space–time symmetric. This behaviour is similar to the experimental space–time asymmetry observed by Nishimura *et al.* (1991) for wavy-walled channels and is in essence a three-dimensional structure as opposed to a two-dimensional breaking of the space–time symmetry.

4.1.2. *Asymmetry*

Asymmetry in the (x, y)-plane is observed to develop at an oscillatory Reynolds number of between 150 and 200. Figure 8 shows a sequence of streakline photographs in the (x, y)-plane at three successive flow reversals for $Re = 250$, $St = 1.0$. A large dominating asymmetric eddy is clearly evident at each flow reversal. The asymmetric flow patterns are observed to be qualitatively similar at all Strouhal numbers studied. Video observations show that although these flows appear periodic over a single cycle, there is a tendency for the flow to wander, so that after 10 cycles or more a different flow pattern may be observed. Thus the level of asymmetry in a flow can vary considerably, from a highly asymmetric flow (as in figure 8) to a flow that is nearly symmetric.

During each oscillation the dominating eddy is observed to drive the mainstream of the flow onto opposite walls during each half-cycle of the flow. This is most clearly evident at higher oscillatory Reynolds numbers. Figure 9 shows streakline photographs in the (x, y)-plane at two successive flow reversals for $Re = 750$, $St = 0.341$. The asymmetric motion in this regime is observed to be remarkably stable over a number of cycles, despite the overall complexity of the flow. Streakline photographs taken at successive periods indicate that the large-scale structures are highly periodic.

(*a*)

(*b*)

(*c*)

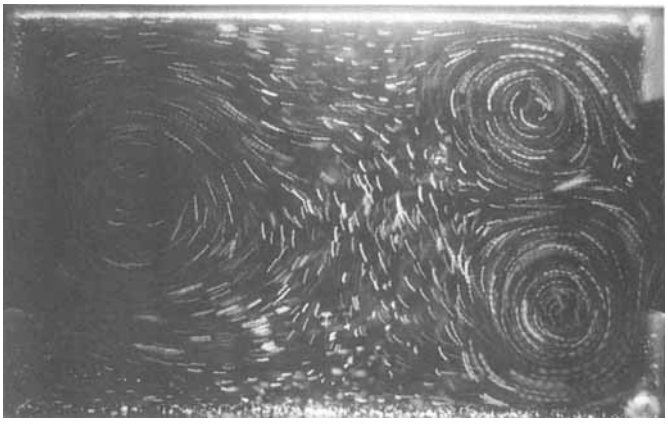

FIGURE 8. A sequence of streakline photographs showing the typical structure of an asymmetric flow. The photographs were taken at three successive flow reversals using a plane of light in the centre of the channel in the (x, y)-plane with an exposure time of 1/15 s. *Re* and *St* were 250 and 1.0 respectively. (*a*) $t = t_0$ (an integer), (*b*) $t = t_0 + 0.5$ and (*c*) $t = t_0 + 1.0$.

(*a*)

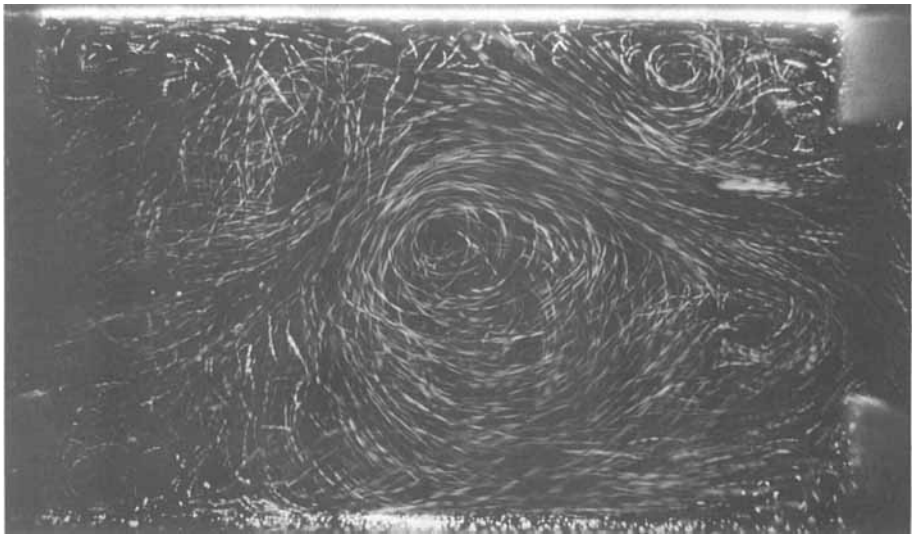

(*b*)

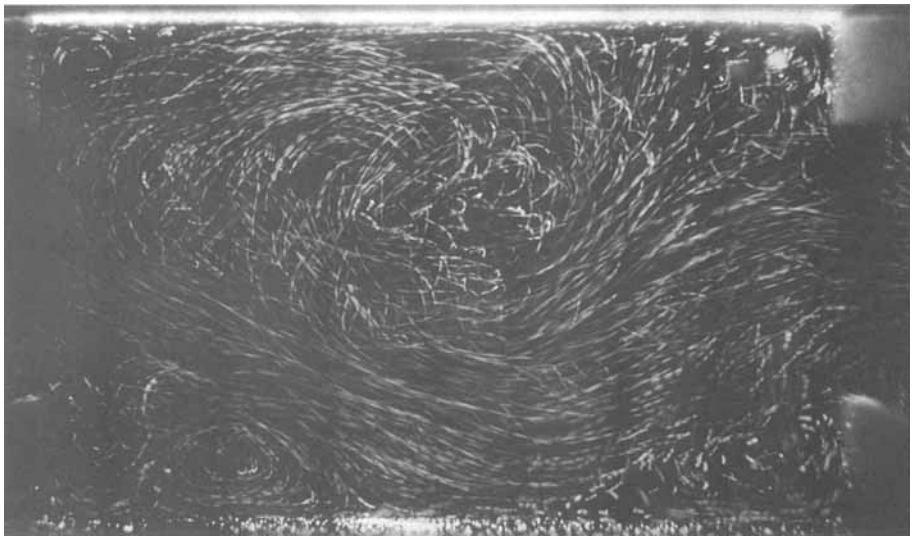

FIGURE 9. A sequence of streakline photographs showing the flow structure at a relatively large Reynolds number. The photographs were taken at two successive flow reversals using a plane of light in the centre of the channel in the (x, y)-plane with an exposure time of 1/30 s. *Re* and *St* were 250 and 1.0 respectively. (*a*) $t = t_0$ (an integer) and (*b*) $t = t_0 + 0.5$.

4.2. *Transitions observed using the numerical simulation*

The experimental observations indicate that the flow becomes three-dimensional at a relatively low oscillatory Reynolds number and direct comparison with the simulation is no longer possible. However, a number of interesting features observed using the numerical simulation do follow the qualitative experimental behaviour and merit more

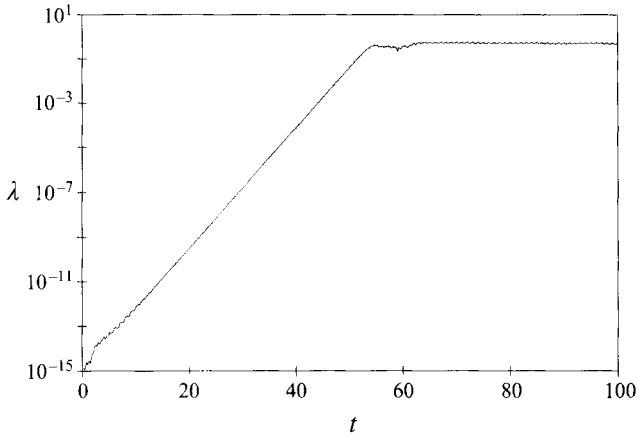

FIGURE 10. The development of asymmetry. The flow was modelled using a two-dimensional numerical simulation and the level of asymmetry monitored using the parameter λ, defined in (13). The initial value of λ is associated with numerically generated truncation errors. The flow is unstable to asymmetric perturbation and there is a linear phase of growth ($t = 0$ to 50). The flow reaches a fully developed saturated asymmetric state for $t > 70$. *Re* and *St* were 160 and 1.0 respectively.

detailed attention. It is also possible that the two-dimensional stability behaviour plays an important role in the transitions observed in the full three-dimensional flow. In plane Poiseuille flow for example, the two-dimensional instability (Tollmien–Schlichting waves), which occurs at a relatively large Reynolds number, is thought to play a part in the transition to three-dimensional flow which is observed experimentally at a lower Reynolds number (Orszag & Kells 1980). Furthermore it is possible that the regimes of two-dimensional flows may be related to oscillatory flows in similar geometries, for example the wavy-walled tube. The development of asymmetry and period-doubling behaviour are therefore explored in detail using the numerical simulation.

4.2.1. *Asymmetry*

If the centreline symmetry constraint is relaxed asymmetric perturbations can grow and lead to asymmetric flows at long times. The level of asymmetry can be quantified using a parameter λ – the mean absolute value of the cross-channel velocity on the centreline (v_c):

$$\lambda = \int_0^L \frac{|v_c|}{L} \mathrm{d}x. \tag{13}$$

This parameter has been used by Roberts (1994) to study the transition to asymmetric flow for constant volumetric flow within a baffled channel.

The flow at $St = 1.0$ is observed to become unstable to asymmetric perturbations at $Re = 93$. Figure 10 shows the behaviour of λ for $Re = 160$, $St = 1.0$. At $t = 0$ λ is of order 10^{-15}, corresponding to the size of truncation errors in the data. Initially there is a linear phase of exponential growth, before nonlinear effects become significant after around 50 oscillation cycles. After 65 cycles the flow reaches a saturated asymmetric state. Figure 11 shows a sequence of instantaneous streamline plots through one cycle of the fully developed flow. The asymmetry is in the form of a dominating eddy which drives the mainstream of the flow onto opposite walls during each half-cycle of the flow. Two eddies are formed during each half-cycle, though one

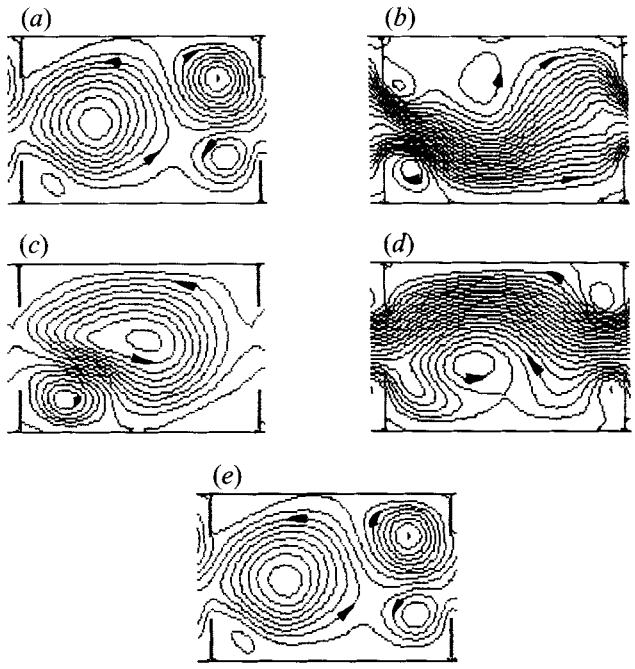

FIGURE 11. A time sequence of plots of instantaneous streamlines in the (x,y)-plane for a fully developed, asymmetric sinusoidal oscillatory flow. A two-dimensional numerial simulation was used to obtain the streamfunction distribution. *Re* and *St* were 160 and 1.0 respectively. Streamfunction ψ is plotted at intervals of 0.05. The flow patterns should be compared with the streakline photographs of figure 8, which show the form of asymmetry which is observed experimentally. (*a*) $t = t_0$ (an integer), (*b*) $t = t_0+0.25$, (*c*) $t = t_0+0.5$, (*d*) $t = t_0+0.75$, and (*e*) $t = t_0+1.0$.

of these merges with the dominating eddy before the point of flow reversal. The dominating eddy survives indefinitely, driven by the asymmetric flow during each half-cycle of the oscillation.

The asymmetric flow patterns observed using the numerical simulation (figure 11) are very similar to those observed experimentally (figure 8). This is in spite of the fact that the experimental flow is three-dimensional and is apparently aperiodic. This agreement in the form of the asymmetry observed in the two cases suggests that the mechanism for transition to asymmetry observed experimentally is associated with the two-dimensional instability, identified with the numerical simulation.

This bifurcation from a symmetric to an asymmetric flow is a pitchfork bifurcation. The space–time symmetry of the flow is broken, and the dominating eddy may be either clockwise or anticlockwise.

At higher oscillatory Reynolds number similar asymmetric flows are observed, with the size and strength of the dominating eddy increasing. The same trends are observed for all values of Strouhal number studied. The Strouhal number influences the shape of the dominating eddy, but the same form of asymmetric flow patterns is observed in all cases. Plots of instantaneous streamlines for a range of Strouhal number have been published in a separate paper (Roberts & Mackley 1995). The critical oscillatory Reynolds number for asymmetry increases with decreasing Strouhal number. By observing the eigenvalue for the instability as it becomes positive it is possible to determine the critical Reynolds number (Re_c) at each value of the Strouhal number. Table 2 shows the value of the critical oscillatory Reynolds number at the four values of Strouhal number studied.

St	Re_c
1.0	93
0.68	105
0.453	135
0.341	156

TABLE 2. Critical oscillatory Reynolds number for asymmetry

Although the experimental flows become three dimensional before they become asymmetric, the form of the asymmetry observed is qualitatively similar to the observations from the numerical simulation. Comparison of figure 11 with figure 8 shows a remarkable similarity in the flow patterns observed.

4.2.2. *Periodicity behaviour*

In order to establish if the flow has reached a fully developed state two periodicity numbers are defined. These can be used to establish the frequency of any time-periodic flow regime.

$$\chi_N = \frac{\sum_{i,j} |\psi_{x,y,t} - \psi_{x,y,t-N}|}{\sum_{i,j} |\psi_{x,y,t}|} \times 100\%, \tag{14}$$

$$\chi_{0.5} = \frac{\sum_{i,j} |\psi_{x,y,t} + \psi_{L-x,y,t-0.5}|}{\sum_{i,j} |\psi_{x,y,t}|} \times 100\%, \tag{15}$$

where i,j represents a grid point on the finite-difference grid. χ_N is a measure of the percentage difference between the flow at time t and the flow N cycles earlier. Thus if $\chi_N \to 0$ then the flow is fully repeating over N cycles. For the flows studied in this paper the behaviour of χ_N is observed for $N = 1$ to 16. $\chi_{0.5}$ has been used to indicate whether the flow is space–time symmetric: if $\chi_{0.5} \to 0$ then the flow is space–time symmetric. This is similar to the parameter used by Ralph (1986) to study the breaking of space–time symmetry.

Figure 12 shows the behaviour of χ_1 for the developing asymmetric flow with $Re = 160$, $St = 1.0$. Initially χ_1 falls to a value of below 1%, before rising again to a value of around 50% after 63 cycles. For $t > 65$, χ_1 tends towards zero indicating that the flow reaches a fully developed state which is periodic over one cycle. This is in agreement with the observed fully developed flow patterns shown in figure 11. Figure 10 indicates that the asymmetry of this flow develops during the first 54 oscillation cycles. Initially the flow is symmetric and the early decay in χ_1 corresponds to the periodicity of the symmetric flow. Once the asymmetry has developed the flow shows a complex transitional behaviour for $54 < t < 65$, evident in figures 10 and 12. This may be a transient chaotic behaviour, before the flow develops into a fully periodic flow. For higher oscillatory Reynolds numbers ($Re > 300$) the flow is not observed to reach a periodic state after 100 cycles.

The most interesting features relating to the periodicity of oscillatory flows are observed using the numerical simulation with the constrained symmetric boundary condition (11).

The development of the flow has been followed with increasing oscillatory Reynolds number for constrained symmetric flow at the four values of Strouhal number studied

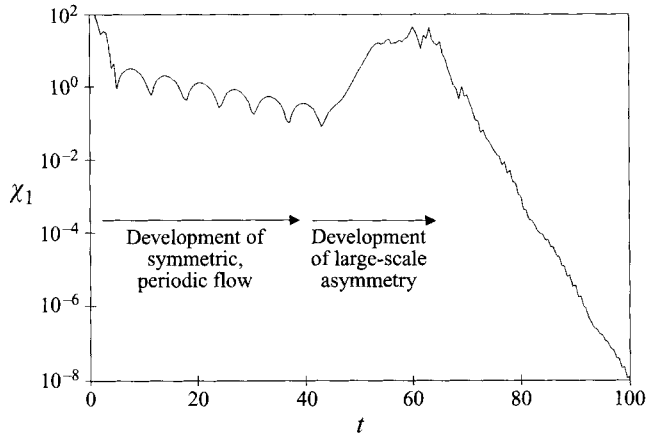

FIGURE 12. The periodicity behaviour for a developing asymmetric flow. The periodicity parameter χ_1 is defined in (14). The flow is followed using a two-dimensional numerical simulation; it is started from rest and the developing periodicity behaviour is associated with the symmetric flow. After around 45 cycles the asymmetric perturbations become large (see figure 10) and the periodicity behaviour changes. After long times, $t > 70$ cycles, χ_1 decays rapidly indicating that the fully developed asymmetric flow is periodic over one oscillation cycle. The flow conditions are identical to those of figure 10 ($Re = 160$, $St = 1.0$) and the fully developed flow patterns are shown in figure 11.

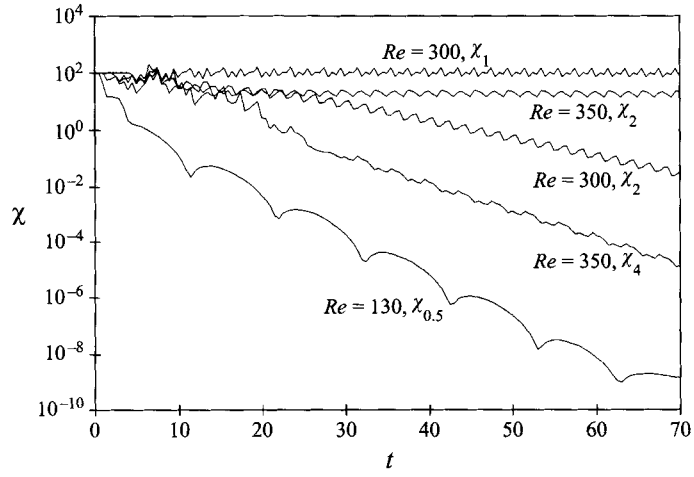

FIGURE 13. The developing periodicity for $St = 1$. The periodicity parameters χ_N and $\chi_{0.5}$ are defined by (14) and (15). If $\chi_N \to 0$ the flow is periodic over N cycles, while if $\chi_{0.5} \to 0$ the flow exhibits space–time symmetry. The flows were followed using a two-dimensional simulation and were constrained to be symmetric. Clearly for $Re = 130$, $\chi_{0.5} \to 0$ and the flow is space–time symmetric. $Re = 300$ and 350, $\chi_2 \to 0$ and $\chi_4 \to 0$, indicating periodicity over two and four cycles respectively.

in this paper. The periodicity parameters $\chi_{0.5}$ and χ_N have been used to characterize this development.

Figure 13 shows the behaviour of periodicity parameters for a range of oscillatory Reynolds numbers with $St = 1.0$. For oscillatory Reynolds numbers of 160 and below the asymptotic flow is observed to be space–time symmetric and fully periodic over each oscillation cycle. In figure 13 the space–time symmetry is clearly indicated for $Re = 130$ by the rapid decay of $\chi_{0.5}$. At an oscillatory Reynolds number between 160 and 200 the flow is observed to pass through a transition from a flow fully repeating over

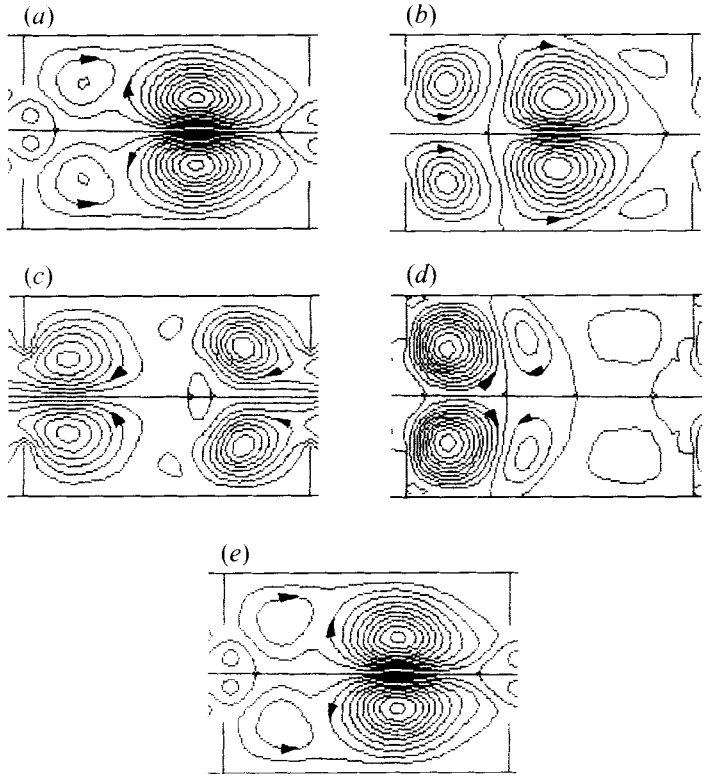

FIGURE 14. A time sequence of plots of instantaneous streamlines in the (x, y)-plane for a fully developed, symmetric sinusoidal oscillatory flow in a baffled channel. A two-dimensional numerical simulation was used to obtain the streamfunction distribution, with the flow constrained to be symmetric. Re and St were 300 and 1.0 respectively. Streamfunction ψ is plotted at intervals of 0.05. Comparison of (*a*) and (*e*) clearly shows that the flow is periodic over two oscillation cycles. (*a*) $t = t_0$ (an integer), (*b*) $t = t_0 + 0.5$, (*c*) $t = t_0 + 1.0$, (*d*) $t = t_0 + 1.5$, and (*e*) $t = t_0 + 2.0$.

one cycle to a flow fully repeating over two cycles. The behaviour of χ_1 and χ_2 is shown in figure 13 for $Re = 300$. χ_1 approaches a positive asymptotic value while χ_2 decays rapidly, indicating that the flow is periodic over two oscillation cycles. Further transitions were observed to flows periodic over four and eight cycles, at oscillatory Reynolds numbers of 300–350 and 370–380 respectively. The behaviour of χ_2 and χ_4 is shown in figure 13 for $Re = 350$. In this case χ_2 approaches a positive asymptotic value while χ_4 decays rapidly, indicating that the flow is periodic over four oscillation cycles

Figure 14 shows the instantaneous streamlines at five successive flow reversals for $Re = 300$, $St = 1.0$ where the flow is periodic over two cycles. This figure suggests that the observed transition is a pitchfork bifurcation as the flows at each flow reversal with $t =$ an integer are very different from those at the opposite flow reversal, with $t =$ an integer $+ 0.5$. Using a different starting boundary condition for the wall streamfunction, a different fully developed flow can be obtained. Replacing (7) and (8) with

$$\text{for } t < 0.5 \quad \psi = 0 \qquad \text{on walls and baffles,} \tag{16}$$

$$\text{for } t > 0.5 \quad \psi = \pm\tfrac{1}{2}\sin(2\pi t) \quad \text{on walls and baffles,} \tag{17}$$

is equivalent to holding the flow stationary for the first half-cycle. The fully developed flow observed using this new starting boundary condition is observed to be the mirror

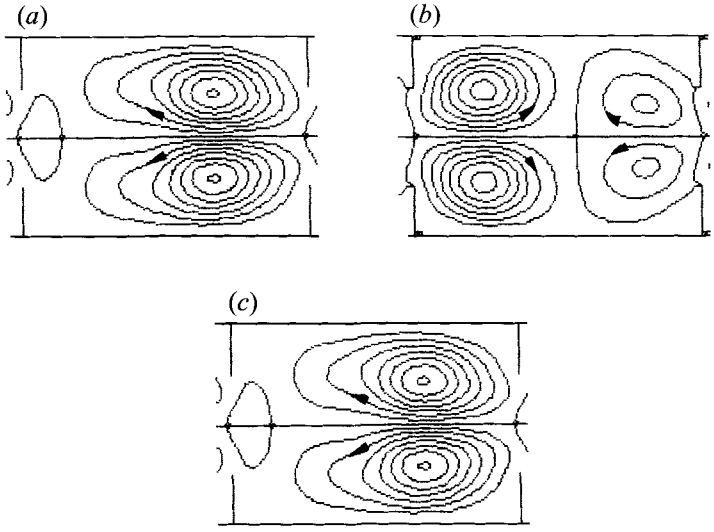

FIGURE 15. As figure 14 but for Re and St were 160 and 0.68 respectively. The space–time symmetry of the flow is broken, but the flow is periodic over one oscillation cycle. (*a*) $t = t_0$ (an integer), (*b*) $t = t_0 + 0.5$, and (*c*) $t = t_0 + 1.0$.

image of the flow shown in figure 14, with the time advanced one half-cycle. Thus two different asymptotic solutions can be obtained, indicating that the observed transition is from a one-cycle repeating flow to two different flows repeating over two cycles (i.e. a period-doubling pitchfork bifurcation).

With $St = 0.68$ the first periodicity transition observed with increasing oscillatory Reynolds number is a breaking of the space–time symmetry of the flow. This transition occurs at $Re = 120$–125. For $Re = 160$ for example, after a development time of thirty cycles, χ_1 falls rapidly, indicating that the fully developed flow is periodic over one cycle. $\chi_{0.5}$ reaches a positive asymptotic value of 65%, indicating that the space–time symmetry of the flow has been broken. Figure 15 shows the flow patterns observed for this fully developed flow at three successive flow reversals. The flow patterns confirm that the space–time symmetry of the flow has been broken.

This bifurcation to space–time asymmetric flow is a pitchfork bifurcation. At higher oscillatory Reynolds numbers with $St = 0.68$ a rapid series of period-doubling bifurcations is observed. Transitions to two-, four-, eight- and sixteen-cycle periodic flows are observed at oscillatory Reynolds numbers of 160–180, 190–195, 195–200 and 200–200.25 respectively.

The sequence of bifurcations described above for $St = 1.0$ and 0.68 is suggestive of a Feigenbaum-like period-doubling cascade that will lead to a chaotic flow regime, where the flow is aperiodic. A universal feature of period-doubling cascades is that the ratio δ_i:

$$\delta_i = \frac{Re_{c,i+1} - Re_{c,i}}{Re_{c,i+2} - Re_{c,i+1}} \tag{18}$$

(where $Re_{c,i}$ is the critical oscillatory Reynolds number for the ith period-doubling bifurcation) tends towards a constant value $\delta = 4.67\ldots$ as i tends to ∞ (see Thompson & Stewart 1986, for example). For the three period-doubling bifurcations observed with $St = 1.0$, $\delta_1 \sim 4$. For $St = 0.68$, we can estimate $\delta_1 \approx 4.5$ and $\delta_2 \approx 4.65$ from the first four period-doubling bifurcations (1 to 2, 2 to 4, 4 to 8 and 8 to 16). These results confirm that the bifurcations observed are indicative of a period-doubling cascade.

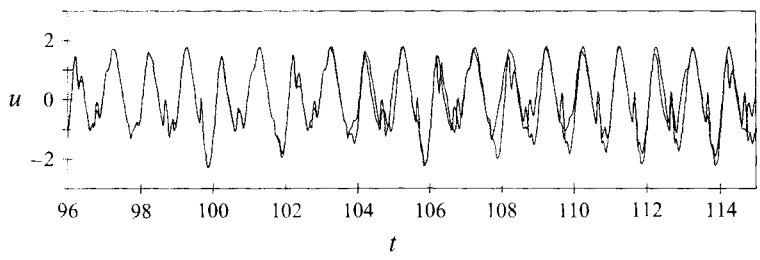

FIGURE 16. Comparison of the trace of the velocity u at a point on the centreline for a perturbed and unperturbed fully developed flow. The flows were followed using a two-dimensional numerical simulation, with the flow constrained to be symmetric. It is clear that the two flows are divergent. The fully developed flow does not appear to be periodic, but some of the oscillating structures of the trace are observed to reappear after a number of oscillation cycles. Re and St were 230 and 0.68 respectively.

From (18) the cascade should be complete at an oscillatory Reynolds number of ~ 390 for $St = 1.0$ and of ~ 201 for $St = 0.68$. For higher oscillatory Reynolds numbers chaotic flows should be observed For both $St = 1.0$ and $St = 0.68$ flows no evidence of periodicity was observed for oscillatory Reynolds numbers greater than 400 and 202 respectively. For these aperiodic flows the velocity at a point on the centreline between the two baffles was observed for many hundreds of oscillations with no evidence of a repeating cycle.

In order to demonstrate that these flows are chaotic it is necessary to show that: (*a*) the flow is sensitive to initial conditions (i.e. there is a positive Liapunov exponent); and (*b*) the fully developed flow is associated with an attractor (specifically a strange attractor). Sensitivity to initial conditions has been demonstrated by introducing a small perturbation to the flow and comparing the subsequent development of the unperturbed and perturbed flows. If the flow is fully developed and chaotic, these flows will diverge at an exponential rate corresponding to the largest Liapunov exponent (see Thompson & Stewart 1986, for example). The magnitude of the initial perturbation used was approximately three orders of magnitude smaller than the residual error in the converged solution at each time step. The perturbation was introduced after 500 oscillation cycles to ensure that the flow had reached a fully developed state. For $St = 0.68$ the flows were found to diverge for Reynolds numbers of $Re > 202$. For these flow conditions the divergence is exponential, indicating that the flow is sensitive to initial conditions and has a positive Liapunov exponent. The rate of divergence was found to increase with oscillatory Reynolds number. At long times, of order 100 cycles, the flows have become significantly different and there is no longer any exponential divergence.

The Liapunov exponent has been estimated from a time sequence of velocity at a point on the centreline using the technique reported by Wolf *et al.* (1985). Estimates of the Liapunov exponent obtained using this technique are in approximate agreement with exponential rate of divergence of the perturbed and unperturbed flows. For example for $Re = 280$, $St = 0.68$ Liapunov exponents of 0.35–0.45 (from the technique of Wolf *et al.* 1985) and 0.39 (from the rate of divergence) are obtained.

Figure 16 shows a trace of the velocity u at a point on the centreline for the unperturbed and perturbed flows with $Re = 230$, $St = 0.68$. The divergence of the flows is clearly evident. It is also evident that although the flow is aperiodic there is a pattern in the trace, in that structures reappear as the flow progresses. This pattern is associated with the structure of the strange attractor for the chaotic flow. The well-known technique of phase-space reconstruction (Packard *et al.* 1980; Thompson &

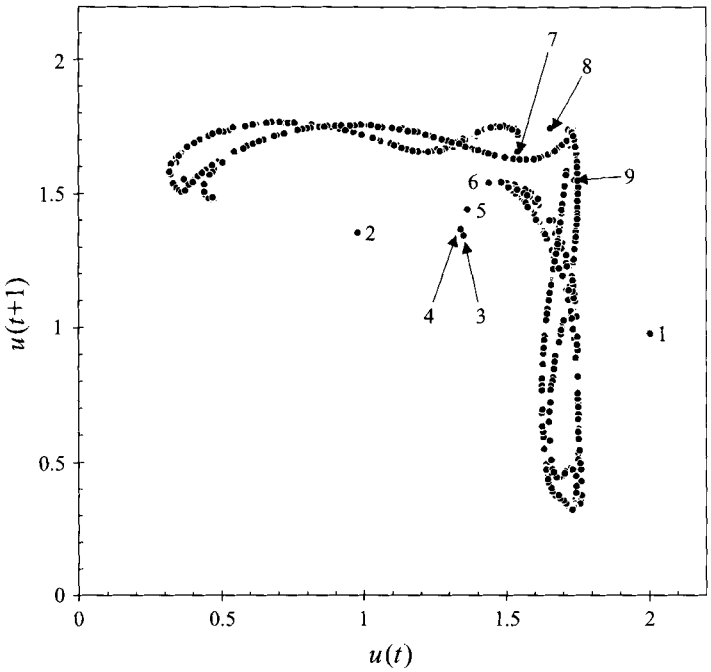

FIGURE 17. A Poincaré map of the trajectory of the velocity u at a point on the centreline in delay coordinates. The flows were followed using a two-dimensional numerical simulation, with the flow constrained to be symmetric; they were started from rest and the points associated with the first nine oscillation cycles are labelled. The structure of the asymptotic attractor is evident from the figure. After only a few oscillation cycles the trajectory rapidly approaches the asymptotic attractor. *Re* and *St* were 230 and 0.68 respectively.

Stewart 1986) can be used to illustrate the structure of an attractor from a time series of data using delay coordinates. Figure 17 shows a Poincaré map of the trajectory of the velocity of a point on the centreline in delay coordinates $[u(t+1)$ versus $u(t)]$ for $Re = 230$, $St = 0.68$. The figure clearly shows that this flow has an associated attractor. The trajectory starts from an initial boundary condition (stationary fluid) which is not associated with the attractor. After only a few oscillation cycles the trajectory rapidly approaches the asymptotic attractor.

For $St = 0.68$ a narrow window of periodic flows occurs at oscillatory Reynolds numbers of $\sim$ 212–216. At $Re = 213$ χ_6 decays towards zero indicating that the flow is periodic over six cycles, while periodicity numbers for fewer oscillations remain high. At $Re = 214$ and 215, $St = 0.68$ observation of the velocity at a point on the centreline for $\sim$ 500 cycles indicates that the flow becomes periodic over 12 and 24 cycles respectively. This suggests that the flow is going through another sequence of period-doubling bifurcations: $6 \rightarrow 12 \rightarrow 24$ etc. This type of behaviour with windows of periodic flows and period-doubling sequences is well known for dynamical systems exhibiting deterministic chaos (e.g. Thompson & Stewart 1986).

A bifurcation diagram has been constructed for increasing oscillatory Reynolds number with $St = 0.68$, using $\chi_{0.5}$ as a parameter (figure 18). This diagram illustrates the sequence of period-doubling cascade leading to chaotic flow. The periodic window observed for $Re = 212$–216 is also shown. It is likely that there are further periodic windows present in the chaotic regions in the bifurcation diagram.

Similar period-doubling sequences are observed for $St = 0.453$ and 0.341. For flows with periodicity greater than one cycle, up to four pairs of eddies are observed at each

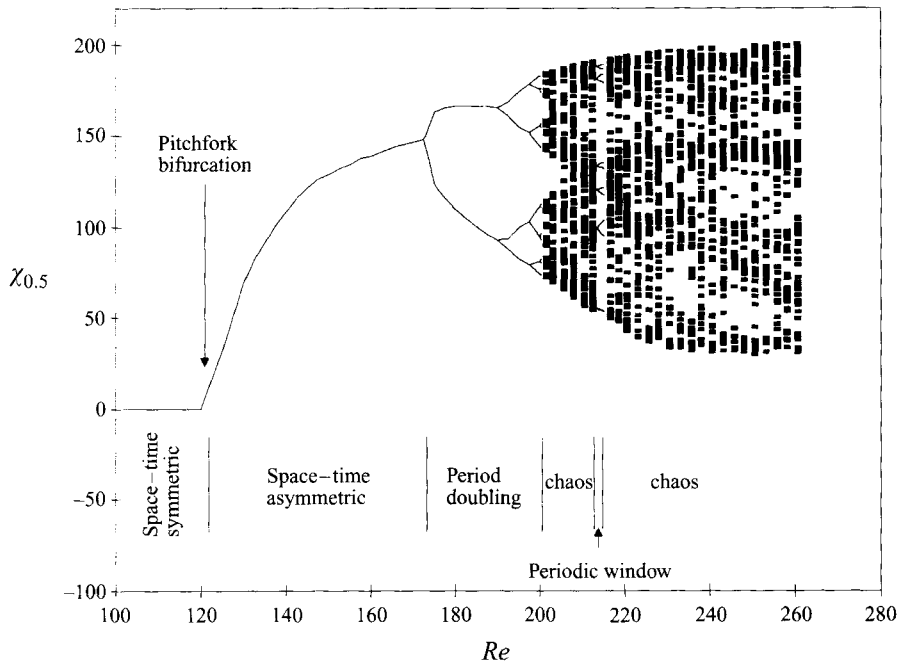

FIGURE 18. The bifurcation diagram for symmetric flow for $St = 0.68$, constructed using a two-dimensional numerical simulation with the flow constrained to be symmetric. The diagram shows how the space–time symmetric flow observed at low Reynolds number develops into a chaotic flow as the oscillatory Reynolds number increases. Note that the flow is observed experimentally to become three-dimensional at an oscillatory Reynolds number of between 100 and 130, and asymmetric for $Re > 200$.

Re	*St* 1.0	0.68	0.453	0.341
1	0.5/1	0.5/1	0.5/1	0.5/1
10	0.5/1	0.5/1	0.5/1	0.5/1
40	0.5/1	0.5/1	0.5/1	0.5/1
80	0.5/2	0.5/2	0.5/1	0.5/1
130	0.5/2	1/2	0.5/2	0.5/1
200	2/2.5	4/2.5	1/1.5	1/1.5
300	2/3.25	∞/2.6	∞/2.1	2/1.75
400	∞/3.3	∞/2.6	∞/2.2	2/2
500		∞/2.8	∞/2.4	

TABLE 3. Periodicity/number of pairs of eddies at flow reversal for constrained symmetric flow. A periodicity of ∞ indicates that no periodicity was observed and the flow is chaotic

flow reversal. The strongest pair of eddies is observed to survive for up to two cycles, while others are formed, merge or disappear during each cycle.

For each Strouhal number the periodicity of the flow has been observed at a range of oscillatory Reynolds numbers. These results are summarized in table 3. Each flow is characterized by two numbers: the first is the number of cycles over which the flow is fully repeating – if the flow is time symmetric this is given as 0.5; the second number is an average number of pairs of eddies in the flow at flow reversal. Increasingly complex flows with a larger number of eddies are observed with increasing oscillatory

Reynolds number. With decreasing Strouhal number at constant oscillatory Reynolds number fewer eddies are observed in each cell.

5. Grid refinement and numerical convergence

The period-doubling cascade observed for the symmetric flows is known to occur in a wide range of nonlinear systems. A number of grid refinement tests have been performed in order to demonstrate that the period doubling is associated with the underlying flow equations rather than the numerical scheme. Grid sizes are quoted as the number of grid points in the x- and y-directions in one inter-baffle cell.

Moore, Weiss & Wilkins (1990) have studied the effect of grid refinement on a period-doubling transition observed for thermosolutal convection. They used a similar Dufort–Frankel leapfrog scheme and showed that when performing grid refinement tests for this scheme it is important to keep $\gamma = Re\,St\Delta t/\Delta x^2$ constant. With γ constant the solution should converge with $\Delta x \rightarrow 0$ with an error proportional to Δx^2. The solution should also converge at any given grid size as $\gamma \rightarrow 0$. A series of tests was therefore performed using grids of (*a*) 32×48, (*b*) 40×64, (*c*) 60×96, (*d*) 80×128 and (*e*) 120×192, while keeping γ constant for all cases. For grids (*a–d*) a bifurcation diagram was constructed which in each case had the same structure as figure 18. For each grid size flows periodic over one, two, four and eight cycles were observed as well as chaotic flows. The critical Reynolds number for each transition was found to be a weak function of the grid size, so that any given Reynolds number the observed flow may depend on the grid size used.

In order to show that the bifurcation structure is convergent the effect of grid size on the critical Reynolds number for the first period-doubling transition has been evaluated for $St = 0.68$. By determining the eigenvalue for the transition as it changes from a negative to positive value it is possible to determine the critical Reynolds number (Re_c) for this transition. Figure 19 shows the effect of grid size on this critical Reynolds number for the grids (*a–e*). The critical Reynolds number is convergent with second-order accuracy on grid spacing, as expected. This confirms that this transition is associated with the two-dimensional Navier–Stokes equations and not with the numerical discretization.

For each refined grid (*b–e*) the periodic window and with a flow of period six was located for oscillatory Reynolds numbers in the range 210–220. The value of the critical Reynolds number for the transition from period-six flow to period-twelve flow was determined in each case. The results suggest that the location of the periodic window is second-order convergent on grid size, but further simulations with finer grids are required to confirm this observation.

The effect of the time step has been evaluated by reducing the time step at a fixed grid size of 40×64. This has the effect of reducing γ with constant Δx. When the time step was reduced from 0.0025 to 0.001 25 the critical Reynolds number for the transition from period-one to period-two flow was affected by less than 1 %. A further reduction in the time step to 0.000 625 gave a change in the critical Reynolds number of less than 0.02 %. The critical Reynolds number is clearly convergent with γ, as expected.

The effect of grid refinement on the transition to asymmetry has also been investigated. Figure 20 shows the behaviour of λ for a flow with $Re = 160$, $St = 1.0$ for a range of grid sizes. In all cases the asymptotic flow is asymmetric and periodic over one oscillation cycle. The transitional behaviour shows some sensitivity to grid size. This is to be expected as the asymmetry develops gradually over some 100 cycles and numerical errors will influence this sensitive transition process. This effect is however

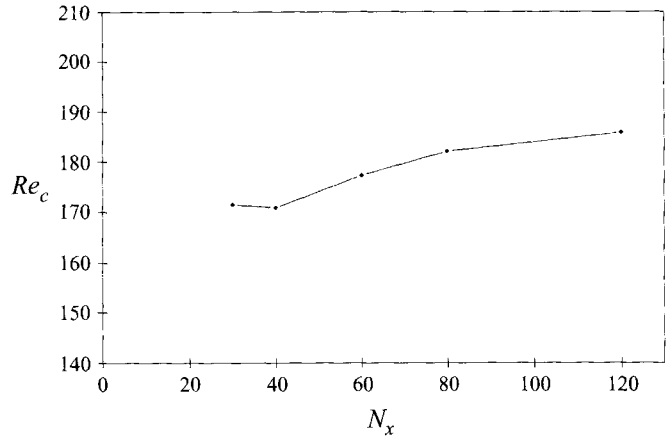

FIGURE 19. The effect of grid size on critical Reynolds number for a period-doubling bifurcation for symmetric flow. Re_c is the critical Reynolds number for the first period-doubling bifurcation calculated using a two dimensional numerical simulation with the flow constrained to be symmetric, for $St = 0.68$. N_x is the number of grid points used in the x-direction, with N_x/N_y and $\gamma = Re\,St\,\Delta t/\Delta x^2$ constant. The figure indicates that Re_c is convergent as $\Delta x \to 0$, and further analysis of the data indicates second-order convergence.

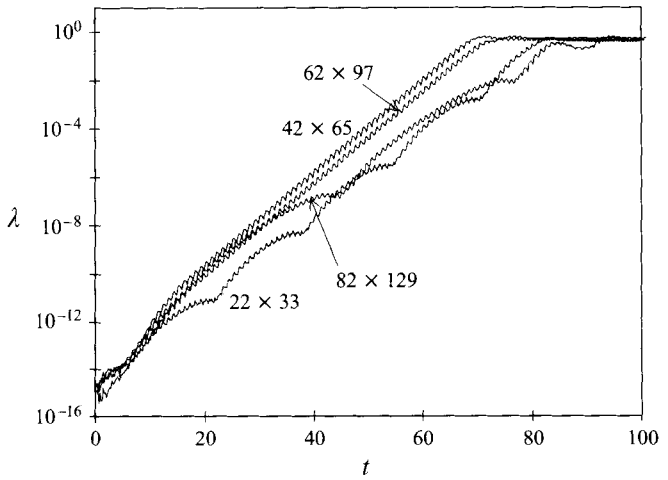

FIGURE 20. The effect of grid size on the development of asymmetry. The flow was started from rest and the level of asymmetry λ followed using a two-dimensional numerical simulation using a range of finite difference grids. The number of grid points used in each case is indicated in the figure.

relatively small and the instability of the symmetric flow is clearly evident for all grid sizes.

5.1. *Spatial periodicity*

The assumption of spatial periodicity for each cell is generally considered to be acceptable for this class of flows. Bernardis, Graham & Parker (1981) studied oscillatory flow through a single orifice plate and observed that very little vorticity was swept back through the orifice when the flow reversed direction. This indicates that the flow in each cell is largely independent of adjacent cells. Thus by modelling the flow as periodic over one cell, a good approximation of the flow field can be obtained even if the flow is observed experimentally to be different in adjacent cells. It is possible to relax the periodicity constraint by observing the effect of varying the number of cells

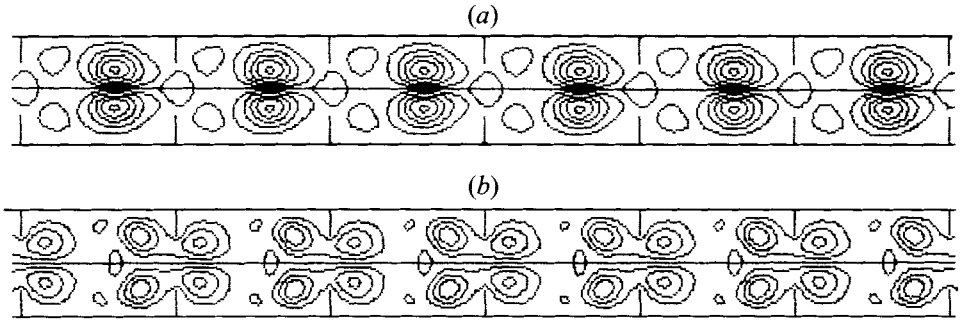

FIGURE 21. A time sequence of plots of instantaneous streamlines in the (x, y)-plane for a fully developed, symmetric flow. A two-dimensional numerical simulation was used to obtain the streamfunction distribution. The flow is constrained to be symmetric and spatially periodic over six cells, as depicted. *Re* and *St* were 300 and 1.0 respectively. Streamfunction ψ is plotted at intervals of 0.1. Comparison with figure 14 indicates that the spatial periodicity assumption has had no effect on the fully developed flow. (*a*) $t = t_0$ (an integer), and (*b*) $t = t_0 + 1.0$.

FIGURE 22. A plot of instantaneous streamlines in the (x, y)-plane for a fully developed, asymmetric sinusoidal flow at the point of flow reversal (t = an integer). A two-dimensional numerical simulation was used to obtain the streamfunction distribution, with the spatial periodicity relaxed to twelve cells, as depicted. The flow was started from rest with a small perturbation to allow differences in the flow in each cell to develop. *Re* and *St* were 200 and 1.0 respectively. Streamfunction ψ is plotted at intervals of 0.1. The flow is periodic over one oscillation cycle, but it is clear from the figure that the flow is not spatially periodic over each cell of the geometry.

modelled on the flow field. Figure 21 shows the fully developed flow patterns for a constrained symmetric flow periodic over six cells for $Re = 300$, $St = 1.0$. The flow was started from rest as normal, and a small perturbation (with a normalized amplitude of order 10^{-5}) introduced at the first time step to give a very slightly different flow in each cell. The converged flow for these conditions was found to be periodic in time over two cycles. Comparison with figures 14(*a*) and 14(*c*) indicates that the assumption of spatial periodicity over one cell does not affect the period-doubling transition.

The effect of the spatial periodicity assumption on the transition to asymmetric flow has also been investigated. Intuitively one might expect that the sense of rotation of the dominating eddy observed would be opposite in adjacent cells, as indicated by the observations of Sobey (1985). In order to observe the effect of spatial periodicity on the asymmetric flows two simulations were carried out with a flow periodic over twelve cells. In the first simulation the solution obtained using a flow periodic over one cell was used as the starting condition in each of the twelve cells. A small perturbation (with a normalized amplitude of order 10^{-5}) was introduced to give a very slightly different flow in each cell. The perturbation was observed to decay exponentially so that the converged solution was identical to the solution assuming periodicity over a single cell. For the second simulation the flow was started from rest, again with a small perturbation (with a normalized amplitude of order 10^{-5}) introduced at the first time step to give a very slightly different flow in each cell. After around 100 cycles the flow was observed to reach a converged solution, periodic over one oscillation cycle. However in this case the flow was not observed to be spatially periodic in each cell. Figure 22 shows the instantaneous streamlines observed at flow reversal. In all but one of the cells a similar flow pattern is observed, with a dominating eddy. The dominating

eddy is rotating counterclockwise in seven cells, clockwise in four cells and in the remaining cell the flow is nearly symmetric. Clearly at least two possible converged solutions are possible, and its seems likely that there may be many more solutions for different spatially periodic boundary conditions. The flow in most of the cells however is very similar to the flow obtained assuming spatial periodicity over a single cell. These observations suggest that the flow in each cell is only a weak function of the flow in adjacent cells.

6. Discussion and conclusions

Experimental observations of cross-channel motions indicate that oscillatory flow in a baffled channel becomes three-dimensional at an oscillatory Reynolds number of order 100 for the range of Strouhal number studied. The cross-channel motion shows a periodic sequence of eddies developing in strength before breaking down into an unstructured three-dimensional flow at $Re \sim 200$. These flow are similar to those observed experimentally by Nishimura *et al.* (1991) for oscillatory flow in wavy-walled channels. Nishimura *et al.* (1991) suggested that this transition was due to a centrifugal (Taylor–Görtler) instability of the line eddy formed at the convex part of the channel wall. Honji (1981) observed a similar three-dimensional instability for flow around an oscillating cylinder. The wavelength of the three-dimensional instability observed by Nishimura *et al.* (1991) is consistent with that observed by Honji (1981) for a cylinder diameter equivalent to the wavelength of the channel wall. Observation of the radius of curvature of the streamlines for the flow patterns observed by Nishimura *et al.* (1991) indicate that this cylinder diameter is reasonable.

Although the wavelengths and form of the flow structure are similar to those observed by Nishimura *et al.* (1991), the trend of increasing wavelength with increasing Strouhal number is opposite to that observed by both Nishimura *et al.* (1991) and Honji (1981). Clearly a three-dimensional perturbation analysis is needed to explain these observations. There is considerable scope for further numerical and experimental studies of these three-dimensional transitions.

The transition to asymmetry observed using the numerical simulation shows remarkable qualitative agreement with the experimentally observed flow patterns (e.g. compare figures 8 and 11). This is in spite of the fact that the experimentally observed flow has a complex three-dimensional structure. The critical oscillatory Reynolds number for transition to three-dimensional flow is found to be close to that observed numerically for the two-dimensional transition to asymmetry. A possible explanation is that the growth rate of symmetric three-dimensional perturbations is much larger than the growth rate of the two-dimensional asymmetric instability. Nonlinear effects could then damp the growth rate of the asymmetric perturbations and retard the transition to asymmetry. The transition to asymmetry may ultimately be associated with the two-dimensional instability, and the comparison with the two-dimensional simulation is consistent with this hypothesis. This may also explain the 'intermittent' behaviour observed under some conditions where the level of asymmetry varied considerably with time. This effect may be a consequence of the two competing flow regimes: three-dimensional symmetric and two-dimensional asymmetric flow. A full three-dimensional simulation or stability study is needed to further evaluate these transitions.

Observations reported in this paper indicate that for numerical simulation of oscillatory flows, care is needed to ensure that a fully developed state has been achieved. In some cases it is necessary to follow many hundreds of oscillation cycles

before the flow is fully developed. This is in contrast to the published literature where oscillations are followed for a development time of order five cycles. It is normal to assume that if the observed flow pattern is nearly identical after successive oscillations the flow is fully developed. The results reported in this paper clearly show that this assumption may not be valid. Very gradual transitions can occur over many oscillation cycles, so that the flow pattern after successive oscillations is nearly identical but after many oscillation cycles the nature of the flow has altered significantly. The use of periodicity numbers to establish the development of the flow has been shown to be a more reliable means of establishing whether the flow is fully developed.

It is natural to assume that the very gradual transitions observed are a consequence of accumulating numerical errors. In this case the period-doubling sequence observed would be an artefact of the numerical scheme and a strong function of the grid size. Grid refinement test indicate that this is not the case and the observed period-doubling sequence is therefore associated with the two-dimensional flow equations.

Experimental observations indicate that the flows studied in this paper become three-dimensional and asymmetric before any period-doubling transitions occur. However, as the first period-doubling transition can be observed at moderate oscillatory Reynolds numbers of order 100–200, it is likely that for some geometries the period-doubling transition will occur before the flow becomes three-dimensional. Indeed the first stage of a period-doubling sequence, the breaking of the space–time symmetry, has been observed experimentally by Ralph (1986). A period-doubling cascade leading to a chaotic flow has been studied by Blondeaux & Vittori (1991) for oscillatory flow over a single wavy wall. Similar behaviour has also been observed by Howes (1988) for oscillatory flow in baffled tubes, although no detailed study was carried out. Period-doubling sequences would seem to be an important mechanism for the development of flow complexity for these types of forced oscillatory flow in obstructed geometries.

Comparison of the observed flow patterns with those presented by Howes (1988) suggests that the toroidal eddies formed in the tube survive for longer than the line eddies observed in this paper. As a consequence of this longevity the flows observed by Howes (1988) show a higher level of complexity than those presented in this paper at equivalent flow conditions. Comparison of the wavy-walled channel flows presented by Sobey (1980, 1983) with the wavy-walled tube flows of Ralph (1986) also shows that the tubular geometry leads to increased flow complexity. Howes (1988) observed experimentally that the flow remained axisymmetrically for oscillatory Reynolds number of up to 300. It would seem likely that for some conditions period doubling may be observed experimentally for oscillatory flow in baffled or wavy walled tubes.

The period-doubling cascade is only one of the possible routes for transition to chaotic flow. Period-doubling sequences have been observed experimentally for some hydrodynamic systems, notably for Rayleigh–Bénard convection (Gollub & Benson 1980). Transition to a chaotic flow regime following a periodic–quasi-periodic–chaotic sequence has been observed for Couette flow by Gollub & Swinney (1975). A period-doubling cascade leading to a chaotic flow has been briefly studied by Blondeaux & Vittori (1991) for an oscillatory flow past a single wavy wall. For oscillatory flow past a cylinder transition to a chaotic regime by the quasi-periodic–phase locking scenario has been observed (Blondeaux & Vittori 1993).

Research into developing flow complexity and the transition to chaotic flow has in the past concentrated on three-dimensional flows or flows for which buoyancy effects are significant. In this paper, a very wide range of flow phenomena and transitions has been observed using a simple two-dimensional simulation for a range of Reynolds

number and Strouhal number conditions. The study of obstructed oscillatory flow offers the opportunity to study developing flow complexity without the need for cumbersome three-dimensional simulation or the introduction of buoyancy effects.

The bifurcation diagram shown in figure 18 clearly shows the developing complexity of the flow. This diagram was constructed from simulation of the fully developed flow rather than from theoretical or stability analysis. This approach provides a powerful tool for following the developing complexity of oscillatory flows. It is important to note that a flow which is chaotic is not necessarily turbulent. In this paper a period-doubling transition to chaotic flow has been observed using a laminar two-dimensional simulation.

There is significant potential for further analysis of the transitions described in the paper. For example in the chaotic region it may be possible to identify further periodic windows. The sequence of periodicity of these windows may correspond to a characteristic sequence such as the U-sequence for one-dimensional maps (e.g. Thompson & Stewart 1986). It is also possible that the characteristics of the flow (i.e. the bifurcation diagram) may be followed using a simple deterministic model with only a few degrees of freedom.

REFERENCES

BELLHOUSE, B. J., BELLHOUSE, F. H., CURL, C. M., MACMILLAN, T. I., GUNNING, A. J., SPRATT, E. H., MACMURRAY, S. B. & NELEMS, J. M. 1973 A high efficiency membrane oxygenator and pulsatile pumping system and its application to animal trials. *Trans. Am. Soc. Artif. Int. Organs* **19**, 77.

BERNARDIS, B. DE, GRAHAM, J. M. R. & PARKER, K. H. 1981 Oscillatory flow around discs and through orifices. *J. Fluid Mech.* **102**, 279.

BLONDEAUX, P. & VITTORI, G. 1991 A route to chaos in an oscillatory flow – Feigenbaum scenario. *Phys. Fluids* A **3**, 2492.

BLONDEAUX, P. & VITTORI, G. 1993 Quasiperiodicity and phase locking route to chaos in the 2-D oscillatory flow around a circular cylinder. *Phys. Fluids* A **5**, 1866.

BRUNOLD, C. R., HUNNS, J. C. B., MACKLEY, M. R. & THOMPSON, J. W. 1989 Experimental observation on flow patterns and energy losses for oscillatory flow in ducts containing sharp edges. *Chem. Engng Sci.* **44**, 1227.

DICKENS, A. W., MACKLEY, M. R. & WILLIAMS, H. R. 1989 Experimental residence time distribution measurements for unsteady flow in a baffled channel. *Chem. Engng Sci.* **44**, 1471.

GOLLUB, J. P. & BENSON, S. H. 1980 Many routes to turbulent convection. *J. Fluid Mech.* **100**, 449.

GOLLUB, J. P. & SWINNEY, H. L. 1975 Onset of turbulence in a rotating fluid. *Phys. Rev. Lett.* **35**, 927.

HEWGILL, M. R., MACKLEY, M. R., PANDIT, A. B. & PANNU, S. S. 1993 Enhancement of gas-liquid mass transfer using pulsed flow in a baffled tube. *Chem. Engng Sci.* **48**, 799.

HONJI, H. 1981 Streaked flow around an oscillating circular cylinder. *J. Fluid Mech.* **107**, 509.

HOWES, T. 1988 Dispersion and unsteady flow in baffled tubes. PhD thesis, Department of Chemical Engineering, University of Cambridge.

HOWES, T., MACKLEY, M. R. & ROBERTS, E. P. L. 1991 The simulation of chaotic mixing and dispersion for periodic flows in baffled channels. *Chem. Engng Sci.* **46**, 1669.

MACKLEY, M. R., TWEDDLE, G. M. & WYATT, I. D. 1990 Experimental heat transfer measurements for pulsatile flow in a baffled tube. *Chem. Engng Sci.* **45**, 1237.

NISHIMURA, T., MIYASHITA, H., MURAKAMI, S. & KAWAMURA, Y. 1991 Oscillatory flow in a symmetric sinusoidal wavy walled channel at intermediate Strouhal numbers. *Chem. Engng Sci.* **46**, 771.

MOORE, D. R., WEISS, N. O. & WILKINS, J. M. 1990 The reliability of numerical experiments: transitions to chaos in thermosolutal convection. *Nonlinearity* **3**, 997.

ORSZAG, S. A. & KELLS, L. C. 1980 The transition to turbulence in plane Poiseuille flow and plane Couette flow. *J. Fluid Mech.* **96**, 159.

PACKARD, N. H., CRUTCHFIELD, J. P., FARMER, J. D. & SHAW, R. S. 1980 Geometry from a time series. *Phys. Rev. Lett.* **45**, 712.

PARK, J. R. S. & BAIRD, M. H. I. 1970 Transition phenomena in an oscillating manometer. *Can. J. Chem. Engng* **48**, 491.

RALPH, M. E. 1986 Oscillatory flow in wavy walled tubes. *J. Fluid Mech.* **168**, 515.

RALPH, M. E. & PEDLEY, T. J. 1986 Flow in a channel with a moving indentation. *J. Fluid Mech.* **190**, 87.

ROACHE, P. J. 1976 *Computational Fluid Dynamics.* Hermosa.

ROBERTS, E. P. L. 1992 Unsteady flow and mixing in baffled channels. PhD thesis, Department of Chemical Engineering, University of Cambridge.

ROBERTS, E. P. L. 1994 A numerical and experimental study of transition processes in an obstructed channel flow. *J. Fluid Mech.* **260**, 185.

ROBERTS, E. P. L. & MACKLEY, M. R. 1995 The simulation of stretch rates for the quantitative prediction and mapping of mixing within a channel flow. *Chem. Engng Sci.* **50**, 3727.

SOBEY, I. J. 1980 On flow through furrowed channels. Part 1. Calculated flow patterns. *J. Fluid Mech.* **96**, 1.

SOBEY, I. J. 1983 The occurrence of separation in oscillatory flow. *J. Fluid Mech.* **134**, 247.

SOBEY, I. J. 1985 Observation of waves during oscillatory channel flow. *J. Fluid Mech.* **151**, 395.

STEPANHOFF, K. D., SOBEY, I. J. & BELLHOUSE, B. J. 1980 On flow through furrowed channels. Part 2. Observed flow patterns. *J. Fluid Mech.* **96**, 27.

THOMPSON, J. M. T. & STEWART, H. B. 1986 *Nonlinear Dynamics and Chaos.* Wiley.

WOLF, A., SWIFT, J. B., SWINNEY, H. L. & VASTANO, J. 1985 Determining Liapunov exponents from a time series. *Physica* **16D**, 285.